8-1-2014

A partition of unity method for the displacement obstacle problem of clamped Kirchhoff plates

Susanne C. Brenner
Louisiana State University

Christopher B. Davis
Louisiana State University

Li Yeng Sung
Louisiana State University

Recommended Citation

Brenner, S., Davis, C., & Sung, L. (2014). A partition of unity method for the displacement obstacle problem of clamped Kirchhoff plates. *Journal of Computational and Applied Mathematics, 265*, 3-16. https://doi.org/10.1016/j.cam.2013.09.033

Journal of Computational and Applied Mathematics 265 (2014) 3–16

Contents lists available at ScienceDirect

Journal of Computational and Applied Mathematics

journal homepage: www.elsevier.com/locate/cam

A partition of unity method for the displacement obstacle problem of clamped Kirchhoff plates☆

Susanne C. Brenner*, Christopher B. Davis, Li-yeng Sung

Department of Mathematics and Center for Computation and Technology, Louisiana State University, Baton Rouge, LA 70803, United States

ARTICLE INFO

Article history:
Received 28 November 2012
Received in revised form 4 September 2013

MSC:
65K15
65N30

Keywords:
Partition of unity method
Displacement obstacle
Clamped Kirchhoff plate
Fourth order
Variational inequality

ABSTRACT

A partition of unity method for the displacement obstacle problem of clamped Kirchhoff plates is considered in this paper. We derive optimal error estimates and present numerical results that illustrate the performance of the method.

1. Introduction

Let Ω be a bounded polygonal domain $\Omega \subset \mathbb{R}^2, f \in L_2(\Omega), g \in H^4(\Omega)$, and $\psi_1, \psi_2 \in C^2(\Omega) \cap C(\bar{\Omega})$ be two obstacle functions such that

$$\psi_1 < \psi_2 \quad \text{in } \Omega \quad \text{and} \quad \psi_1 < g < \psi_2 \quad \text{on } \partial\Omega. \tag{1.1}$$

Consider the following problem: find $u \in H^2(\Omega)$ such that

$$u = \operatorname*{argmin}_{v \in K} G(v), \tag{1.2}$$

where

$$K = \{v \in H^2(\Omega) : v - g \in H_0^2(\Omega), \psi_1 \le v \le \psi_2 \text{ on } \Omega\}, \tag{1.3}$$

$$G(v) = \frac{1}{2}a(v, v) - (f, v), \tag{1.4}$$

$$a(v, w) = \int_\Omega \nabla^2 v : \nabla^2 w \, dx, \qquad (f, v) = \int_\Omega f v \, dx \tag{1.5}$$

and $\nabla^2 v : \nabla^2 w = \sum_{i,j=1}^2 v_{x_i x_j} w_{x_i x_j}$ is the (Frobenius) inner product of the Hessian matrices of v and w.

☆ The work of the first and third authors was supported in part by the National Science Foundation under Grant Nos. DMS-10-16332 and DMS-13-19172. The work of the second author was supported in part by the National Science Foundation through the VIGRE Grant 07-39382.

* Corresponding author.
E-mail addresses: brenner@math.lsu.edu (S.C. Brenner), cdav135@lsu.edu (C.B. Davis), sung@math.lsu.edu (L.-y. Sung).

0377-0427/$ – see front matter © 2013 Elsevier B.V. All rights reserved.
http://dx.doi.org/10.1016/j.cam.2013.09.033

Since K is a nonempty closed convex subset of $H^2(\Omega)$ and $a(\cdot,\cdot)$ is symmetric and coercive on $H_0^2(\Omega)$ which contains the set $K-K=\{v-w : v, w \in K\}$, it follows from the standard theory [1–4] that (1.2) has a unique solution $u \in K$ characterized by the following variational inequality:

$$a(u, v-u) \geq (f, v-u) \quad \forall v \in K. \tag{1.6}$$

The convergence of finite element methods for second order obstacle problems was investigated in [5–7], shortly after it was shown in [8] that the solutions for such obstacle problems belong to $H^2(\Omega)$ under appropriate regularity assumptions on the data. This full elliptic regularity allows the complementarity form of the variational inequality (in the strong sense) to be used in the convergence analysis.

In contrast, the solutions of fourth order obstacle problems do not belong to $H^4_{loc}(\Omega)$ even if all the data are smooth [9]. It was shown in [10,11,9] that the solution u of (1.2)/(1.6) belongs to $H^3_{loc}(\Omega) \cap C^2(\Omega)$ under the assumptions above on f, g, ψ_1 and ψ_2. Since the obstacles are separated from each other and from the displacement boundary condition (cf. (1.1)), we have $\Delta^2 u = f$ near $\partial\Omega$. Therefore it follows from the elliptic regularity theory for the biharmonic operator on polygonal domains [12–15] that $u \in H^{2+\alpha}(\mathcal{N})$ for some $\alpha \in (\frac{1}{2}, 2]$ in an open neighborhood $\mathcal{N}$ of $\partial\Omega$. The elliptic regularity index α is determined by the interior angles of Ω and we can take α to be 1 for convex Ω. Thus the solution u of (1.2)/(1.6) belongs to $H^{2+\alpha}(\Omega) \cap H^3_{loc}(\Omega) \cap C^2(\Omega)$ in general.

This lack of $H^4_{loc}(\Omega)$ regularity means that the complementarity form of (1.6) only exists in a weak sense, and the convergence analysis based on the second order approach would only lead to suboptimal error estimates.

A new convergence analysis for finite element methods for (1.2)/(1.6) that does not rely on the complementarity form of the variational inequality (1.6) was proposed in [16], where optimal convergence was established for C^1 finite element methods, classical nonconforming finite element methods, and C^0 interior penalty methods for clamped plates ($g = 0$) on convex domains. The results in [16] were subsequently extended to general polygonal domains and general Dirichlet boundary conditions for a quadratic C^0 interior penalty method [17] and a Morley finite element method [18]. The goal of this paper is to extend the results in [17,18] to a partition of unity method (PUM) for plates [19,20].

The rest of the paper is organized as follows. We introduce the partition of unity method in Section 2 and carry out the convergence analysis in Section 3. Numerical results are reported in Section 4, followed by some concluding remarks in Section 5.

2. A partition of unity method

We begin with the construction of the approximation space V_h in Section 2.1 and define an interpolation operator from $H^2(\Omega)$ into V_h in Section 2.2. The discrete obstacle problem is given in Section 2.3. We refer the readers to [21,22] for various aspects of generalized finite element methods.

2.1. Construction of the approximation space

The approximation space is based on partition of unity by flat-top functions [23–25].

2.1.1. Partition of unity

Let ϕ be the C^1 piecewise polynomial function given by

$$\phi(x) = \begin{cases} \phi^L(x) := (1+x)^2(1-2x) & \text{if } x \in [-1, 0] \\ \phi^R(x) := (1-x)^2(1+2x) & \text{if } x \in [0, 1] \\ 0 & \text{if } |x| \geq 1, \end{cases}$$

which enjoys the partition of unity property that

$$\phi^L(x-1) + \phi^R(x) = 1 \quad \text{for } 0 \leq x \leq 1. \tag{2.1}$$

We define a flat-top function ψ_δ by

$$\psi_\delta(x) = \begin{cases} \phi^L\left(\dfrac{x-(-1+\delta)}{2\delta}\right) & \text{if } x \in [-1-\delta, -1+\delta] \\ 1 & \text{if } x \in [-1+\delta, 1-\delta] \\ \phi^R\left(\dfrac{x-(1-\delta)}{2\delta}\right) & \text{if } x \in [1-\delta, 1+\delta] \\ 0 & \text{if } x \notin [-1-\delta, 1+\delta]. \end{cases}$$

Here δ is a small number that controls the width of the flat-top part of this function where $\psi_\delta = 1$.

For ease of presentation we take Ω to be a rectangle $(a, b) \times (c, d)$. But the construction and analysis can be extended to other domains (cf. Remark 2.4 and Examples 4.4 and 4.5 in Section 4).

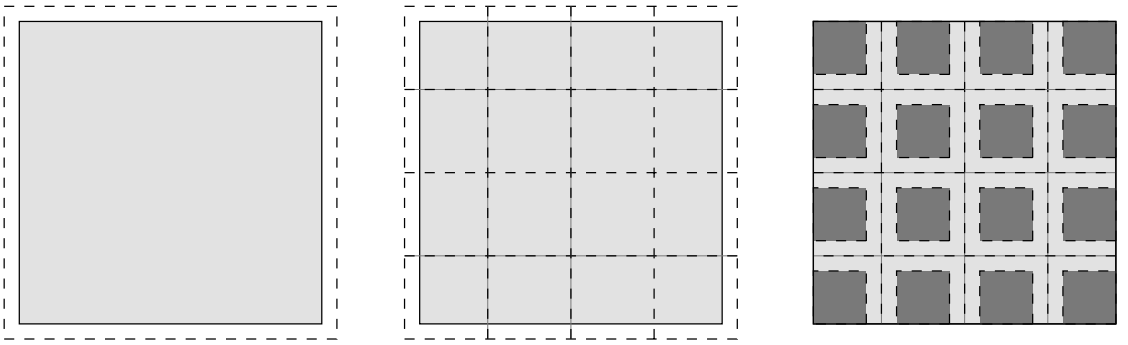

Fig. 2.1. Partitioning of a square domain Ω: first we expand the shaded region Ω to $\tilde{\Omega}$ (left). Next we divide $\tilde{\Omega}$ into congruent rectangles Q_j, $1 \le j \le 16$ (middle). The flat top regions Q_j^{flat}, $1 \le j \le 16$ are shown as the darker shaded regions (right).

We first expand Ω to a larger rectangle $\tilde{\Omega} = (a-\gamma_1, b+\gamma_1) \times (c-\gamma_2, d+\gamma_2)$ where γ_1 and γ_2 are two positive numbers, and then we divide $\tilde{\Omega}$ into disjoint congruent closed rectangular patches Q_j (cf. Fig. 2.1) with center $y_j = (y_{j,1}, y_{j,2})$, width h_1 and height h_2, for $j = 1, \ldots, N$. We assume that the numbers $\delta_j = \gamma_j/(h_j/2)$ $(j = 1, 2)$ satisfy

$$\beta_1 \le \delta_j \le \beta_2, \tag{2.2}$$

where β_1 and β_2 are constants such that $0 < \beta_1 < \beta_2 < 1$.

For each patch Q_j, let

$$\Psi_j(x) = \psi_{\delta_1}\left(\frac{x_1 - y_{j,1}}{h_1/2}\right)\psi_{\delta_2}\left(\frac{x_2 - y_{j,2}}{h_2/2}\right).$$

It follows from (2.1) that $\{\Psi_j, j = 1, \ldots, N\}$ is a partition of unity in Ω, i.e.,

$$\sum_{j=1}^{N} \Psi_j = 1 \quad \text{on } \Omega.$$

The flat-top region of each patch, defined by

$$Q_j^{\text{flat}} = \{x \in Q_j : \Psi_j(x) = 1\},$$

is the rectangle centered at y_j with width $h_1(1-\delta_1) = h_1 - 2\gamma_1$ and height $h_2(1-\delta_2) = h_2 - 2\gamma_2$ (cf. Fig. 2.1).

Remark 2.1. By construction we have (cf. Fig. 2.1)

- $Q_j^{\text{flat}} \cap Q_i^{\text{flat}} = \emptyset$ if $i \ne j$.
- The support of Ψ_j extends a horizontal distance of $\gamma_1 = \delta_1(h/2)$ and a vertical distance of $\gamma_2 = \delta_2(h/2)$ outside of the patch Q_j. Hence the supports for Ψ_i and Ψ_j will intersect in a rectangular region of width $2\gamma_1$ or $2\gamma_2$ if Q_i is a neighbor of Q_j.
- If $Q_j \cap \partial\Omega \ne \emptyset$, then $Q_j^{\text{flat}} \cap \partial\Omega \ne \emptyset$.

Remark 2.2. The overlapping rectangles obtained by expanding each nonoverlapping rectangle Q_i by the amount of γ_1 in the $\pm x_1$ direction and the amount of γ_2 in the $\pm x_2$ direction are the ones usually referred to as patches in the literature for partition of unity methods. They are precisely the supports of the partition of unity functions Ψ_i $(1 \le i \le N)$.

2.1.2. Approximation space

The space $\mathbb{Q}_2$ of biquadratic polynomials will serve as the local approximation space and the global approximation space is defined to be

$$V_h = \left\{\sum_{j=1}^{N} p_j\Psi_j : p_j \in \mathbb{Q}_2\right\}.$$

Below we present an explicit basis of V_h that will be used in our numerical computations.

On the reference interval $[-1, 1]$ we have two types of quadratic polynomials:

- Lagrange interpolation polynomials $L_i(\xi)$ that satisfy $N_i(L_j) = \delta_{ij}$ for $1 \le i, j \le 3$, where $N_1(v) = v(-1)$, $N_2(v) = v(0)$, and $N_3(v) = v(1)$.

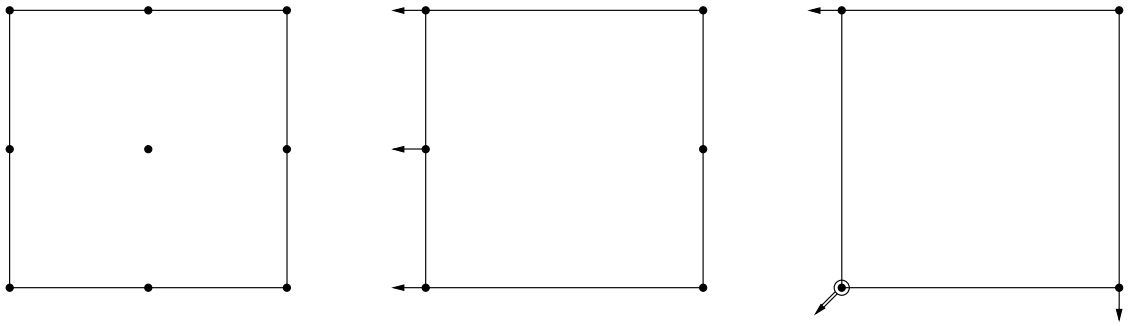

Fig. 2.2. Reference elements described in (2.3)–(2.5) respectively.

- Hermite interpolation polynomials $H_i(\xi)$ that satisfy $N_i(H_j) = \delta_{ij}$ for $1 \le i, j \le 3$, where $N_1(v) = v'(-1), N_2(v) = v(-1)$, and $N_3(v) = v(1)$.

The tensor product of different combinations of these polynomials will provide local bases on the two-dimensional rectangular patches.

Let $T_j : \mathbb{R}^2 \longrightarrow \mathbb{R}^2$ be defined by

$$T_j(\xi_1, \xi_2) = (y_{j,1} + \xi_1(h_1/2)(1 - \delta_1), y_{j,2} + \xi_2(h_2/2)(1 - \delta_2)).$$

Then T_j maps the reference square $[-1, 1] \times [-1, 1]$ to the flat-top region Q_j^{flat}.

Depending on the location of the patch Q_j, we use different reference basis functions. There are three possibilities.

- For those patches Q_j that do not intersect $\partial\Omega$, the reference basis functions are

$$\hat{f}_{ji}(\xi) = L_k(\xi_1)L_l(\xi_2), \quad i = 3(l-1) + k,\ 1 \le k, l \le 3. \tag{2.3}$$

- For those patches Q_j that intersect the boundary on only one side, say the vertical edge $x_1 = a$ of Ω, the reference basis functions are

$$\hat{f}_{ji}(\xi) = H_k(\xi_1)L_l(\xi_2), \quad i = 3(l-1) + k,\ 1 \le k, l \le 3. \tag{2.4}$$

Note that in this case T_j maps the line $\xi_1 = -1$ to the part of Q_j that intersects $\partial\Omega$. The cases where Q_j intersects other sides of Ω can be treated analogously.

- For those patches Q_j that intersect a corner of Ω, say the lower left corner (a, c), the reference basis functions are

$$\hat{f}_{ji}(\xi) = H_k(\xi_1)H_l(\xi_2), \quad i = 3(l-1) + k,\ 1 \le k, l \le 3. \tag{2.5}$$

Note that in this case T_j maps the corner $(-1, -1)$ of the reference square to the lower left corner (a, c) of Ω. The cases where Q_j intersects other corners of Ω can be treated analogously.

The nodal variables (or degrees of freedom) for the local approximation space are depicted in Fig. 2.2, where pointwise evaluations of functions, directional derivatives, gradients and mixed second order derivatives are represented by solid dots, arrows, circles and double arrows respectively.

An explicit basis for the global approximation space V_h is then given by

$$\left\{\Psi_j\left[\hat{f}_{ji} \circ T_j^{-1}\right] : j = 1, 2, \ldots, N;\ i = 1, 2, \ldots, 9\right\}. \tag{2.6}$$

Remark 2.3. Since all the nodes in a rectangular patch Q_j are located in Q_j^{flat} where $\Psi_k = 0$ for $k \ne j$, all the basis functions of V_h vanish at the nodes in Q_j except those associated with Q_j.

Fig. 2.3 illustrates the degrees of freedom associated with the basis of the global approximation space for a square which is divided into 9 square patches where $h_1 = h_2 = h$ and $\delta_1 = \delta_2 = \delta$.

Remark 2.4. One may follow the same procedure for non-convex polygonal domains. As an example, consider an L-shaped domain $(-a, a)^2 \setminus [0, a]^2$. One could divide the domain into rectangular patches everywhere except near the reentrant corner. Near the reentrant corner, one could construct local biquadratic polynomial basis functions in the reference L-shaped domain $(-1, 1)^2 \setminus [0, 1]^2$ dual to the nodal variables

$$N_1(v) = v(0, 0), \qquad N_2(v) = v(1, 0), \qquad N_3(v) = v(0, 1),$$

$$N_4(v) = v(-1, -1), \qquad N_5(v) = \frac{\partial v}{\partial \xi_1}(0, 0), \qquad N_6(v) = \frac{\partial v}{\partial \xi_1}(0, 1),$$

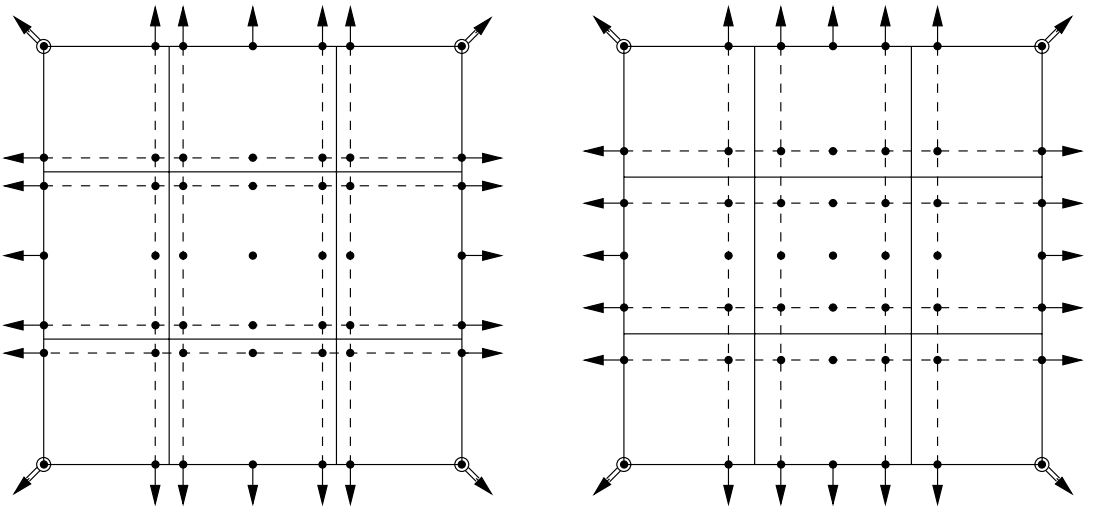

Fig. 2.3. A partition of a domain Ω differing only by the choice of δ. The solid lines separate the different patches $Q_j, j = 1, \ldots, 9$. The dashed lines represent the extension of Q_j by $\delta(h/2)$ on each side. This figure also shows the location of the degrees of freedom corresponding to $\delta = 1/6$ (left) and $\delta = 1/3$ (right).

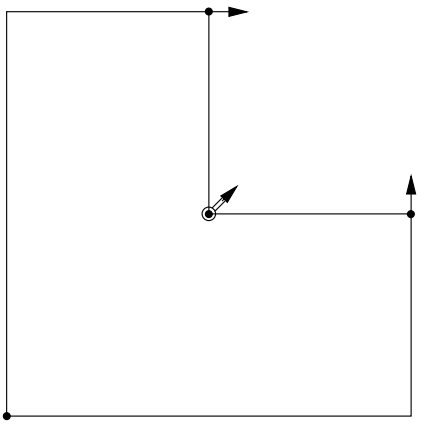

Fig. 2.4. Reference element for the L-shaped domain.

$$N_7(v) = \frac{\partial v}{\partial \xi_2}(0,0), \qquad N_8(v) = \frac{\partial v}{\partial \xi_2}(0,1), \qquad N_9(v) = \frac{\partial^2 v}{\partial \xi_1 \xi_2}(0,0),$$

as depicted in Fig. 2.4.

2.2. Interpolation operator

First we define interpolation operators associated with the rectangular patches. Let $\zeta \in H^2(\mathbb{R}^2)$.

- For a patch with the local basis given by (2.3) (cf. the reference element on the left of Fig. 2.2), we define $\Pi_j\zeta$ to be the polynomial in $\mathbb{Q}_2$ such that $(\Pi_j\zeta) \circ T_j = \zeta \circ T_j$ at the 9 points in the set $\{(p, q) : p, q = -1, 0, 1\}$.
- For a patch with the local basis given by (2.4) (cf. the reference element in the middle of Fig. 2.2), we define $\Pi_j\zeta$ to be the polynomial in $\mathbb{Q}_2$ such that
  (i) $(\Pi_j\zeta) \circ T_j = \zeta \circ T_j$ at the 6 points in the set $\{(p, q) : p = -1, 1 \text{ and } q = -1, 0, 1\}$.
  (ii) The polynomial $(\partial[(\Pi_j\zeta) \circ T_j]/\partial\xi_1)|_{\xi_1=-1}$ equals the quadratic polynomial $\hat{\lambda}(\xi_2)$, which is the L_2 projection of $(\partial(\zeta \circ T_j)/\partial\xi_1)|_{\xi_1=-1}$ into the space of quadratic polynomials in the variable ξ_2.
- For a patch with the local basis given by (2.5) (cf. the reference element on the right of Fig. 2.2), we define $\Pi_j\zeta$ to be the polynomial in $\mathbb{Q}_2$ such that
  (i) $(\Pi_j\zeta) \circ T_j = \zeta \circ T_j$ at the 4 points in the set $\{(p, q) : p, q = \pm 1\}$.
  (ii) $(\partial[(\Pi_j\zeta) \circ T_j]/\partial\xi_1)|_{\xi_1=-1}$ equals the quadratic polynomial $\hat{\lambda}$ at $\xi_2 = \pm 1$, where $\hat{\lambda}(\xi_2)$ is the L_2 projection of $(\partial(\zeta \circ T_j)/\partial\xi_1)|_{\xi_1=-1}$ into the space of quadratic polynomials in the variable ξ_2.

(iii) $(\partial[(\Pi_j\zeta)\circ T_j]/\partial\xi_2)|_{\xi_2=-1}$ equals the quadratic polynomial $\hat{\mu}$ at $\xi_1 = \pm 1$, where $\hat{\mu}(\xi_1)$ is the L_2 projection of $(\partial(\zeta\circ T_j)/\partial\xi_2)|_{\xi_2=-1}$ into the space of quadratic polynomials in the variable ξ_1.

(iv) The value of $(\partial^2[(\Pi_j\zeta)\circ T_j]/\partial\xi_1\partial\xi_2)$ at $(-1,-1)$ equals $(\hat{\lambda}'(-1)+\hat{\mu}'(-1))/2$.

Remark 2.5. Since T_j maps the reference square to Q_j^{flat}, the interpolant $\Pi_j\zeta$ is determined by the restriction of ζ to Q_j^{flat}.

We can now define the global interpolation operator $\Pi_h : H^2(\Omega) \longrightarrow V_h$ by

$$\Pi_h\zeta = \sum_{j=1}^{N}(\Pi_j\zeta_\dagger)\Psi_j \quad \forall\zeta\in H^2(\Omega),$$

where $\zeta_\dagger \in H^2(\mathbb{R}^2)$ is any extension of ζ. The interpolant Π_h is independent of the choice of $\zeta_\dagger$ by Remark 2.5. Moreover, by construction we have

$$\Pi_h(H_0^2(\Omega)) = V_h\cap H_0^2(\Omega). \tag{2.7}$$

Let $\tilde{Q}_j$ be the rectangle centered at y_j with width $h_1(1+\delta_1) = h_1+2\gamma_1$ and height $h_2(1+\delta_2) = h_2+2\gamma_2$. Let $h = \max(h_1,h_2)$. Since $\Pi_j P = P$ for any $P\in\mathbb{Q}_2$, the estimate

$$\sum_{m=0}^{2} h^m|\zeta-\Pi_j\zeta|_{H^m(\tilde{Q}_j\cap\Omega)} \le Ch^{2+\alpha}|\zeta|_{H^{2+\alpha}(\tilde{Q}_j\cap\Omega)} \tag{2.8}$$

follows from the Bramble–Hilbert lemma [26,27] and scaling. From here on we use C to denote a generic positive constant that is independent of the mesh size h.

Combining the local interpolation error estimate (2.8) and the estimates for the partition of unity functions Ψ_j in [25], we immediately have (cf. [24,25]) the following error estimates for the global interpolation operator Π_h:

$$\sum_{m=0}^{2} h^m|\zeta-\Pi_h\zeta|_{H^m(\Omega)} \le Ch^{2+\alpha}|\zeta|_{H^{2+\alpha}(\Omega)}, \tag{2.9}$$

where C depends on the constant β_1 in (2.2).

Remark 2.6. Classical rectangular C^1 finite element methods would require a local approximation space that is at least bi-cubic [28]. Of course we can also use bi-cubic polynomials as the local approximation space in our PUM (cf. [19,20] and Example 1 in Section 4).

2.3. The discrete obstacle problem

Let $\mathcal{V}_h$ be the set of the nodes in the rectangular patches corresponding to the degrees of freedom involving pointwise evaluation of the local basis functions. (Such nodes are represented by solid dots in Figs. 2.3 and 2.4.) The PUM for the model problem is to find $u_h\in K_h$ such that

$$u_h = \operatorname*{argmin}_{v\in K_h} G(v), \tag{2.10}$$

where the quadratic functional G is defined by (1.4)–(1.5) and

$$K_h = \{v\in V_h : v-\Pi_h g\in H_0^2(\Omega),\ \psi_1(p)\le v(p)\le\psi_2(p)\forall p\in\mathcal{V}_h\}. \tag{2.11}$$

Remark 2.7. Approximation of the essential boundary conditions $u = g$ and $\partial u/\partial n = \partial g/\partial n$ are both included in the definition of K_h. Moreover K_h is nonempty because $\Pi_h K\subset K_h$ by (1.3) and (2.7).

Remark 2.8. In view of Remark 2.3 and the defining properties of the polynomials L_i and H_i, the constraints defining K_h are box constraints with respect to the basis of V_h defined in (2.6).

It follows from the standard theory that the discrete obstacle problem (2.10) has a unique solution characterized by the discrete variational inequality

$$a(u_h, v-u_h)\ge(f, v-u_h) \quad \forall v\in K_h. \tag{2.12}$$

3. Convergence analysis

We begin with some preliminary estimates in Section 3.1 and introduce an auxiliary obstacle problem in Section 3.2 that connects the continuous problem (1.2) and the discrete problem (2.10). The main result is derived in Section 3.3.

3.1. Preliminary estimates

In view of (2.9), it suffices to find an optimal estimate for $|\Pi_h u - u_h|_{H^2(\Omega)}$. Using the discrete variational inequality (2.12), we have

$$\begin{aligned}|\Pi_h u - u_h|^2_{H^2(\Omega)} &= a(\Pi_h u - u, \Pi_h u - u_h) + a(u - u_h, \Pi_h u - u_h)\\ &\le |\Pi_h u - u|_{H^2(\Omega)}|\Pi_h u - u_h|_{H^2(\Omega)} + a(u, \Pi_h u - u_h) - (f, \Pi_h u - u_h)\\ &\le \frac{1}{2}|\Pi_h u - u|^2_{H^2(\Omega)} + \frac{1}{2}|\Pi_h u - u_h|^2_{H^2(\Omega)} + a(u, \Pi_h u - u_h) - (f, \Pi_h u - u_h),\end{aligned}$$

which implies

$$|\Pi_h u - u_h|^2_{H^2(\Omega)} \le |\Pi_h u - u|^2_{H^2(\Omega)} + 2\left[a(u, \Pi_h u - u_h) - (f, \Pi_h u - u_h)\right]. \tag{3.1}$$

We can therefore complete the error analysis by finding an optimal estimate for the expression $a(u, \Pi_h u - u_h) - (f, \Pi_h u - u_h)$.

The following result is useful for the error analysis in Section 3.3.

Lemma 3.1. *There exists a positive constant C independent of h such that*

$$|a(\phi, \zeta - \Pi_h\zeta)| \le Ch^{2\alpha}\|\phi\|_{H^{2+\alpha}(\Omega)}\|\zeta\|_{H^{2+\alpha}(\Omega)} \tag{3.2}$$

for all $\phi \in H^{2+\alpha}(\Omega)$ and $\zeta \in H^{2+\alpha}(\Omega) \cap H^2_0(\Omega)$.

Proof. Let $\zeta \in H^{2+\alpha}(\Omega) \cap H^2_0(\Omega)$ be arbitrary. On the one hand we have an obvious estimate

$$\begin{aligned}|a(\phi, \zeta - \Pi_h\zeta)| &\le |\phi|_{H^2(\Omega)}|\zeta - \Pi_h\zeta|_{H^2(\Omega)}\\ &\le Ch^{\alpha}|\phi|_{H^2(\Omega)}|\zeta|_{H^{2+\alpha}(\Omega)} \quad \forall \phi \in H^2(\Omega)\end{aligned} \tag{3.3}$$

that follows from (2.9). On the other hand, we have another estimate

$$\begin{aligned}|a(\phi, \zeta - \Pi_h\zeta)| &= \left|\int_\Omega (\nabla\cdot\nabla^2\phi)\cdot\nabla(\zeta - \Pi_h\zeta)\,dx\right|\\ &\le C|\phi|_{H^3(\Omega)}|\zeta - \Pi_h\zeta|_{H^1(\Omega)}\\ &\le Ch^{1+\alpha}|\phi|_{H^3(\Omega)}|\zeta|_{H^{2+\alpha}(\Omega)} \quad \forall \phi \in H^3(\Omega)\end{aligned} \tag{3.4}$$

that follows from (2.7) and (2.9) and integration by parts.

The estimate (3.2) follows from (3.3) and (3.4) and interpolation between Sobolev spaces [29,30]. □

3.2. An auxiliary obstacle problem

We can connect the continuous obstacle problem (1.2) and the discrete obstacle problem (2.10) through an intermediate obstacle problem: Find $\tilde{u}_h \in \tilde{K}_h$ such that

$$\tilde{u}_h = \operatorname*{argmin}_{v\in\tilde{K}_h} G(v) \tag{3.5}$$

where

$$\tilde{K}_h = \{v \in H^2(\Omega) : v - g \in H^2_0(\Omega),\ \psi_1(p) \le v(p) \le \psi_2(p) \forall p \in \mathcal{V}_h\}. \tag{3.6}$$

Note that $\tilde{K}_h$ is a closed convex subset of $H^2(\Omega)$ and $K \subset \tilde{K}_h$. The unique solution of (3.5) is characterized by the variational inequality:

$$a(\tilde{u}_h, v - \tilde{u}_h) \ge (f, v - \tilde{u}_h) \quad \forall v \in \tilde{K}_h. \tag{3.7}$$

The connection between (1.2) and (3.5) is given by the following properties of $\tilde{u}_h$ from [16,17]:

$$|u - \tilde{u}_h|_{H^2(\Omega)} \le Ch, \tag{3.8}$$

and there exists $h_0 > 0$ such that

$$\hat{u}_h = \tilde{u}_h + \delta_{h,1}\phi_1 - \delta_{h,2}\phi_2 \in K \quad \forall h \le h_0, \tag{3.9}$$

where ϕ_1 and ϕ_2 are nonnegative C^∞ functions with compact supports in Ω such that $\phi_i = 1$ on the coincidence set $\{x \in \Omega : u(x) = \psi_i(x)\}$, and the positive numbers $\delta_{h,1}$ and $\delta_{h,2}$ satisfy

$$\delta_{h,i} \le Ch^2. \tag{3.10}$$

Note that $v - \Pi_h g \in H^2_0(\Omega)$ for all $v \in K_h$ (cf. (2.11)) and hence, by (3.6),

$$v + (g - \Pi_h g) \in \tilde{K}_h \quad \forall v \in K_h. \tag{3.11}$$

3.3. Error estimates for the partition of unity method

We now complete the error analysis of the partition of unity method by deriving an optimal estimate for the expression $a(u, \Pi_h - u_h) - (f, \Pi_h u - u_h)$. To simplify the presentation, we introduce the transitive relation $A \underset{\cdot}{\leq} B$ defined by

$$A \underset{\cdot}{\leq} B \Leftrightarrow A \leq B + C(h^{2\alpha} + h^{\alpha}|\Pi_h u - u_h|_{H^2(\Omega)}).$$

Since

$$a(u, \Pi_h u - u_h) = a(u - \tilde{u}_h, \Pi_h u - u_h) + a(\tilde{u}_h, \Pi_h u - u_h)$$

and

$$a(u - \tilde{u}_h, \Pi_h u - u_h) \leq |u - \tilde{u}_h|_{H^2(\Omega)}|\Pi_h u - u_h|_{H^2(\Omega)} \leq Ch|\Pi_h u - u_h|_{H^2(\Omega)}$$

by the estimate (3.8), we have

$$a(u, \Pi_h u - u_h) - (f, \Pi_h u - u_h) \underset{\cdot}{\leq} a(\tilde{u}_h, \Pi_h u - u_h) - (f, \Pi_h u - u_h). \tag{3.12}$$

In view of (3.11), we can use the auxiliary variational inequality (3.7) to obtain

$$\begin{aligned} a(\tilde{u}_h, \Pi_h u - u_h) &= a(\tilde{u}_h, \tilde{u}_h - u_h - (g - \Pi_h g)) + a(\tilde{u}_h, \Pi_h u - \tilde{u}_h + (g - \Pi_h g)) \\ &\leq (f, \tilde{u}_h - u_h - (g - \Pi_h g)) + a(\tilde{u}_h, \Pi_h u - \tilde{u}_h + (g - \Pi_h g)), \end{aligned}$$

which together with (3.12) implies

$$\begin{aligned} a(u, \Pi_h u - u_h) - (f, \Pi_h u - u_h) &\underset{\cdot}{\leq} a(\tilde{u}_h, \Pi_h u - \tilde{u}_h + (g - \Pi_h g)) \\ &\quad - (f, u - \tilde{u}_h) - (f, (\Pi_h u - u) + (g - \Pi_h g)). \end{aligned} \tag{3.13}$$

We can rewrite the first term on the right-hand side of (3.13) as

$$a(\tilde{u}_h, \Pi_h u - \tilde{u}_h + (g - \Pi_h g)) = a(\tilde{u}_h - u, \Pi_h u - \tilde{u}_h + (g - \Pi_h g)) + a(u, \Pi_h(u - g) - (u - g)) + a(u, u - \tilde{u}_h).$$

Observe that

$$\begin{aligned} a(\tilde{u}_h - u, \Pi_h u - \tilde{u}_h + (g - \Pi_h g)) &= a(\tilde{u}_h - u, (\Pi_h u - u) + (u - \tilde{u}_h) + (g - \Pi_h g)) \\ &\leq |\tilde{u}_h - u|_{H^2(\Omega)} \left(|\Pi_h u - u|_{H^2(\Omega)} + |u - \tilde{u}_h|_{H^2(\Omega)} + |g - \Pi_h g|_{H^2(\Omega)}\right) \\ &\leq Ch^{1+\alpha} \end{aligned}$$

by (2.9) and (3.8), and

$$a(u, \Pi_h(u - g) - (u - g)) \leq Ch^{2\alpha}$$

by Lemma 3.1. Moreover we have, by (2.9),

$$-(f, (\Pi_h u - u) + (g - \Pi_h g)) \leq \|f\|_{L_2(\Omega)} \left(\|\Pi_h u - u\|_{L_2(\Omega)} + \|g - \Pi_h g\|_{L_2(\Omega)}\right) \leq Ch^{2+\alpha}.$$

Combining these relations and (3.13), we arrive at the estimate

$$a(u, \Pi_h u - u_h) - (f, \Pi_h u - u_h). \underset{\cdot}{\leq} a(u, u - \tilde{u}_h) - (f, u - \tilde{u}_h). \tag{3.14}$$

According to (1.6), (3.9) and (3.10), we have

$$\begin{aligned} a(u, u - \tilde{u}_h) - (f, u - \tilde{u}_h) &= a(u, u - \hat{u}_h) - (f, u - \hat{u}_h) + \delta_{h,1}[a(u, \phi_1) - (f, \phi_1)] - \delta_{h,2}[a(u, \phi_2) - (f, \phi_2)] \\ &\leq Ch^2, \end{aligned}$$

and hence (3.14) leads to the estimate

$$a(u, \Pi_h u - u_h) - (f, \Pi_h u - u_h) \underset{\cdot}{\leq} 0,$$

which means

$$a(u, \Pi_h u - u_h) - (f, \Pi_h u - u_h) \leq C(h^{2\alpha} + h^{\alpha}|\Pi_h u - u_h|_{H^2(\Omega)}). \tag{3.15}$$

Theorem 3.2. *There exists a positive constant C independent of h (but dependent on the constant β_1 in (2.2)) such that*

$$|u - u_h|_{H^2(\Omega)} \leq Ch^{\alpha}.$$

Proof. It follows from (2.9), (3.1) and (3.15) and the arithmetic and geometric means inequality that

$$|\Pi_h u - u_h|^2_{H^2(\Omega)} \leq C(h^{2\alpha} + h^{\alpha}|\Pi_h u - u_h|_{H^2(\Omega)}) \leq Ch^{2\alpha} + \frac{1}{2}|\Pi_h u - u_h|^2_{H^2(\Omega)},$$

Table 4.1
Energy norm and ℓ_∞ norm errors for Example 4.1.

j	$\|e_j\|_j/\|u_8\|_8$	β_h	$\|e_j\|_\infty$	β_∞
1	0.0000×10^{-0}		0.0000×10^{-0}	
2	1.2365×10^{-1}		8.8312×10^{-4}	
3	6.3226×10^{-2}	0.9094	6.0088×10^{-4}	0.5221
4	2.5977×10^{-2}	1.2447	8.8401×10^{-5}	2.6817
5	1.2159×10^{-2}	1.0787	2.4443×10^{-5}	1.8267
6	5.9045×10^{-3}	1.0343	6.7946×10^{-6}	1.8331
7	2.9125×10^{-3}	1.0157	1.4775×10^{-6}	2.1929
8	1.4396×10^{-3}	1.0147	8.8608×10^{-7}	0.7363

which implies

$$|\Pi_h u - u_h|_{H^2(\Omega)} \leq Ch^\alpha. \tag{3.16}$$

The theorem follows from (2.9) and (3.16) and the triangle inequality. □

Since $H^2(\Omega)$ is embedded in $C(\bar{\Omega})$ by the Sobolev embedding theorem [29,30], the following corollary is immediate. But numerical results in Section 4 indicate that the convergence rate in the $L_\infty(\Omega)$ norm should be higher than the convergence rate in the $H^2(\Omega)$ norm.

Corollary 3.3. *There exists a positive constant C independent of h such that*

$$|u - u_h|_{L_\infty(\Omega)} \leq Ch^\alpha. \tag{3.17}$$

Remark 3.4. Under additional assumptions [31,32] on the exact coincidence sets (resp. free boundaries), the error estimate (3.17) implies the convergence of the discrete coincidence sets (resp. free boundaries) to the exact coincidence sets (resp. free boundaries). Details can be found in [17].

4. Numerical results

We present numerical results for several one-obstacle problems to demonstrate the performance of the PUM. The obstacle function from below will be denoted by ψ. The first four examples are from [17]. The discrete obstacle problems are solved by a primal dual active set strategy from [33,34].

Example 4.1. Here we apply the PUM to a problem with a known exact solution to validate the numerical results. We begin with the plate obstacle problem on the disk $\{x : |x| < 2\}$ with $f = 0$, $\psi(x) = 1 - |x|^2$ and homogeneous Dirichlet boundary conditions. This problem is rotationally invariant and can be solved exactly. The exact solution is

$$u(x) = \begin{cases} C_1|x|^2 \ln|x| + C_2|x|^2 + C_3 \ln|x| + C_4 & \text{for } r_0 < |x| < 2 \\ 1 - |x|^2 & \text{for } |x| \leq r_0, \end{cases}$$

where $r_0 \approx 0.18134452$, $C_1 \approx 0.52504063$, $C_2 \approx -0.62860904$, $C_3 \approx 0.01726640$, and $C_4 \approx 1.04674630$. We then consider the obstacle problem on $\Omega = (-0.5, 0.5)^2$ whose exact solution is the restriction of u to Ω. For this problem $f = 0$, $\psi(x) = 1 - |x|^2$ and the (non-homogeneous) Dirichlet boundary data are determined by u.

We partition Ω following the procedure described in Section 2.1 and define j to be the level where there are 2^j equal subdivisions in each direction. We solve the discrete obstacle problem on each level j with $\delta = 1/3$ so that the mesh parameter $h_j = (2^j - 1/3)^{-1}$.

We denote the energy norm on the j-th level by $\|\cdot\|_j$. Let u_j be the numerical solution of the j-th level discrete obstacle problem and $e_j = \Pi_j u - u_j$, where Π_j is the interpolation operator on the j-th level. We evaluate the error $\|e_j\|_j$ in the energy norm, and the error $\|e_j\|_\infty$ in the ℓ_∞ norm, and compute the rates of convergence in these norms by

$$\beta_h = \ln(\|e_{j/2}\|_{j/2}/\|e_j\|_j)/\ln(h_{j/2}/h_j) \quad \text{and} \quad \beta_\infty = \ln(\|e_{j/2}\|_\infty/\|e_j\|_\infty)/\ln(h_{j/2}/h_j).$$

The numerical results are presented in Table 4.1. It is observed that the magnitude of the error in energy norm is $O(h)$.

The exact coincidence set I for this example is the disk centered at $(0, 0)$ with radius r_0. Let $\mathcal{V}_j$ be the set of nodes on the j-th level corresponding to degrees of freedom involving pointwise evaluation of local basis functions in the interior of Ω. Then we define the discrete coincidence set I_j by

$$I_j = \{p \in \mathcal{V}_j : u_j(p) - \psi(p) \leq \|e_j\|_\infty\}.$$

The discrete coincidence sets I_7 and I_8 are displayed in Fig. 4.1, where the radius of the circle in black is r_0. The convergence of the discrete coincidence sets is observed.

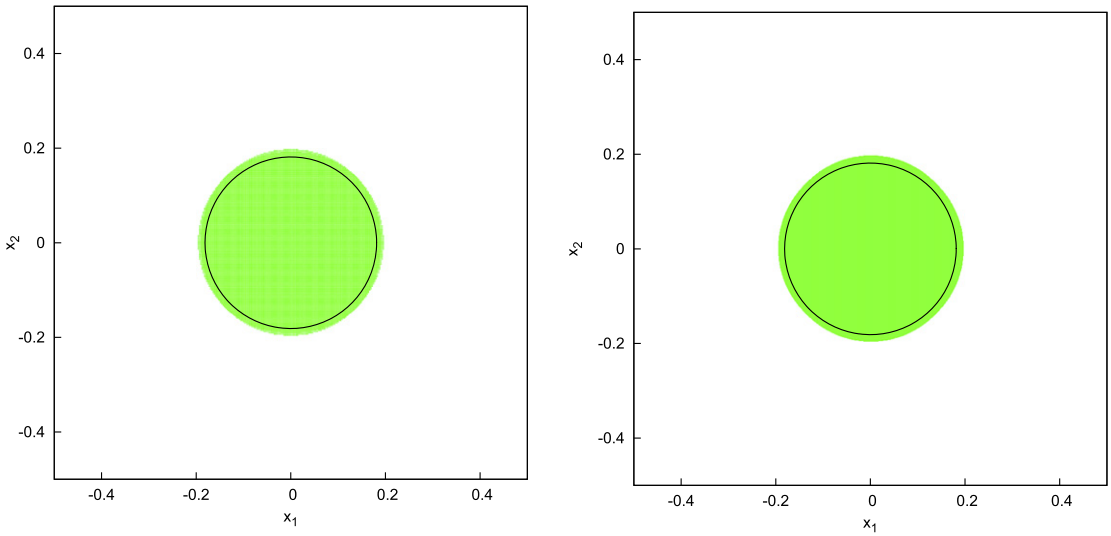

Fig. 4.1. Discrete coincidence set for Example 4.1 for level 7 (left) and level 8 (right).

Table 4.2
Energy norm and ℓ_∞ norm errors for Example 4.1 with $\mathbb{Q}_3$ as local approximation space.

j	$\|e_j\|_j/\|u_7\|_7$	β_h	$\|e_j\|_\infty$	β_∞
1	1.4199×10^{-2}		1.0561×10^{-4}	
2	6.1489×10^{-2}	−1.8589	7.6281×10^{-4}	−2.5078
3	1.8374×10^{-2}	1.6377	9.4507×10^{-5}	2.8313
4	5.8004×10^{-3}	1.6134	1.4396×10^{-5}	2.6330
5	2.3728×10^{-3}	1.2702	4.7114×10^{-6}	1.5872
6	8.3768×10^{-4}	1.4908	4.1685×10^{-7}	3.4723
7	2.7675×10^{-4}	1.5918	3.7129×10^{-6}	−3.1431

Table 4.3
Energy norm and ℓ_∞ norm errors for Example 4.2.

j	$\|\tilde{e}_j\|_j/\|u_8\|_8$	$\tilde{\beta}_h$	$\|\tilde{e}_j\|_\infty$	$\tilde{\beta}_\infty$
1	2.9288×10^{-0}		9.0040×10^{-1}	
2	5.9820×10^{-0}	−0.9058	5.3416×10^{-1}	0.6622
3	1.2402×10^{-0}	2.1333	5.2357×10^{-1}	0.0271
4	6.5242×10^{-1}	0.8988	2.5914×10^{-2}	4.2061
5	1.8496×10^{-1}	1.7913	1.7757×10^{-3}	3.8091
6	8.9273×10^{-2}	1.0430	4.4337×10^{-4}	1.9867
7	4.4296×10^{-2}	1.0072	1.1284×10^{-4}	1.9667
8	2.2154×10^{-2}	0.9977	3.7776×10^{-5}	1.5758

One of the advantages of the PUM is that the local approximation space can be easily adjusted. In Table 4.2 we report the numerical results for the same problem but with $\mathbb{Q}_3$ as the local approximation space. An $O(h^{1.5})$ energy error is observed, which is due to the fact that the exact solution u is piecewise smooth.

Remark 4.1. Note that the ℓ_∞ norm errors fluctuate. This is likely due to the fact that the primal dual active set strategy is based on stopping conditions that are unrelated to the ℓ_∞ norm.

Example 4.2. In this example we take $\Omega = (-0.5, 0.5)^2, f = g = 0$ and $\psi(x) = 1 - 5|x|^2 + |x|^4$. We solve the discrete obstacle problems using the same PU functions as in Example 4.1.

Since the exact solution is not known, we take $\tilde{e}_j = \Pi_j u_{j-1} - u_j$ and compute the rates of convergence $\tilde{\beta}_h$ and $\tilde{\beta}_\infty$ by

$$\tilde{\beta}_h = \ln(\|\tilde{e}_{j/2}\|_{j/2}/\|\tilde{e}_j\|_j)/\ln(h_{j/2}/h_j) \quad \text{and} \quad \tilde{\beta}_\infty = \ln(\|\tilde{e}_{j/2}\|_\infty/\|\tilde{e}_j\|_\infty)/\ln(h_{j/2}/h_j).$$

The results are presented in Table 4.3.

Since $\Delta^2\psi - f > 0$ in this example, the non-coincidence set is known to be connected [9]. This is confirmed by the discrete coincidence sets I_7 and I_8 displayed in Fig. 4.2. Note that the discrete coincidence sets have the correct symmetries: rotations by right angles and reflections across coordinates axes.

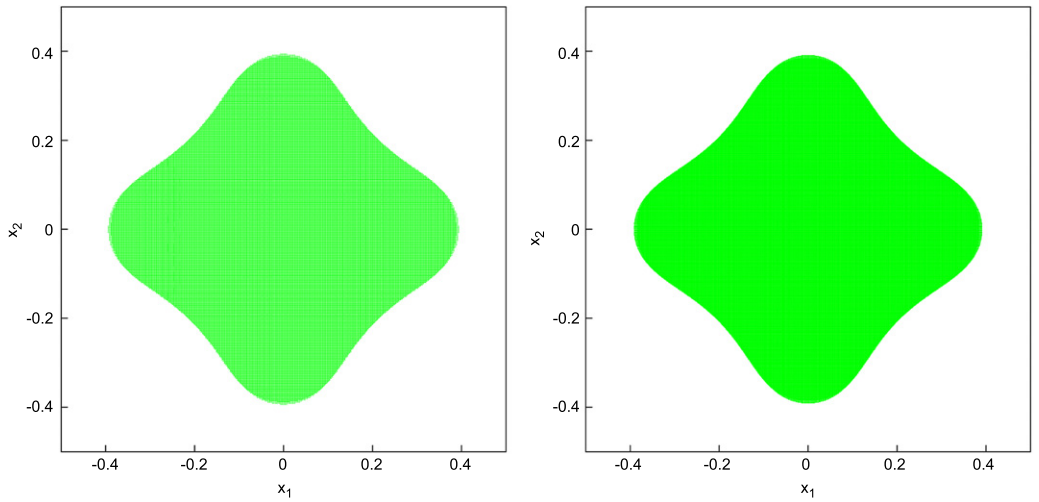

Fig. 4.2. Discrete coincidence set for Example 4.2 for level 7 (left) and level 8 (right).

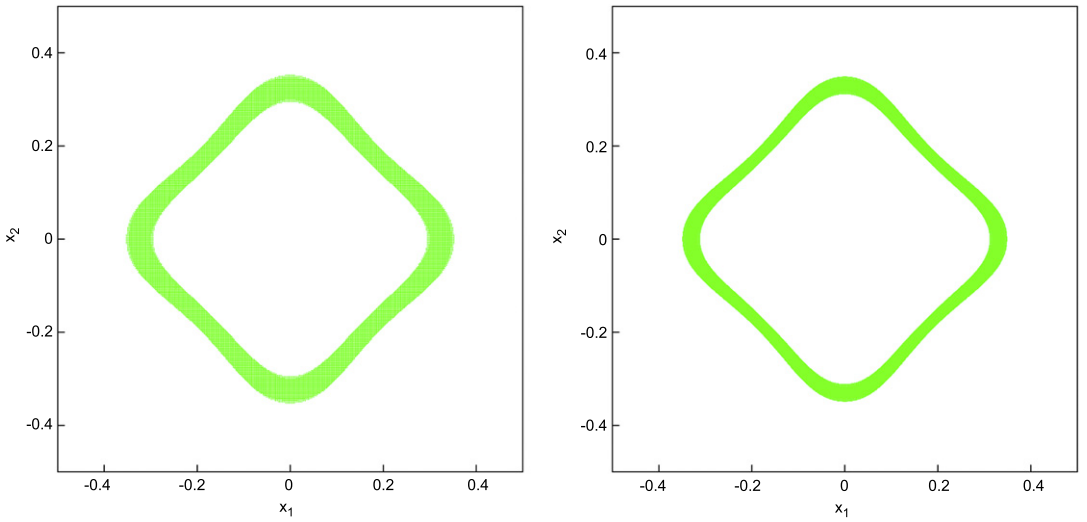

Fig. 4.3. Discrete coincidence set for Example 4.3 for level 7 (left) and level 8 (right).

Table 4.4
Energy norm and ℓ_∞ norm errors for Example 4.3.

j	$\|\tilde{e}_j\|_j / \|u_8\|_8$	$\tilde{\beta}_h$	$\|\tilde{e}_j\|_\infty$	$\tilde{\beta}_\infty$
1	3.0796×10^{-0}		8.9960×10^{-1}	
2	6.2833×10^{-0}	−0.9044	4.8507×10^{-1}	0.7834
3	1.0279×10^{-0}	2.4544	4.3181×10^{-1}	0.1576
4	2.9125×10^{-1}	1.7646	1.9025×10^{-2}	4.3689
5	1.4890×10^{-1}	0.9533	1.6296×10^{-3}	3.4920
6	7.1583×10^{-2}	1.0487	4.8682×10^{-4}	1.7300
7	3.6108×10^{-2}	0.9836	1.3055×10^{-4}	1.8916
8	1.8072×10^{-2}	0.9966	3.1174×10^{-5}	2.0623

Example 4.3. In this example we take $\Omega = (-0.5, 0.5)^2, f = g = 0$ and $\psi(x) = 1 - 5|x|^2 - |x|^4$. We solve the discrete obstacle problems using the same PU functions as in Example 4.1. Numerical results are tabulated in Table 4.4.

The set-up for Example 4.3 is very similar to that of Example 4.2, except that now $\Delta^2\psi - f < 0$ and hence the interior of the coincidence set must be empty, otherwise the complementarity form of the variational inequality would be violated. This is confirmed by the discrete coincidence sets in Fig. 4.3, which also possess the correct symmetries.

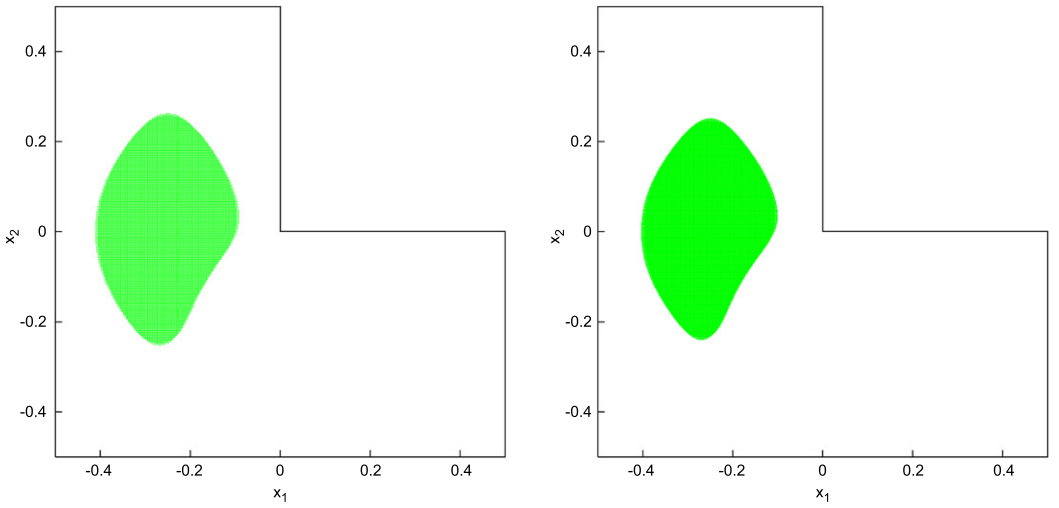

Fig. 4.4. Discrete coincidence set for Example 4.4 for level 7 (left) and level 8 (right).

Table 4.5
Energy norm and ℓ_∞ norm errors for Example 4.4.

j	$\|\tilde{e}_j\|_j/\|u_8\|_8$	$\tilde{\beta}_h$	$\|\tilde{e}_j\|_\infty$	$\tilde{\beta}_\infty$
1	4.4737×10^{-0}		1.0000×10^{-0}	
2	6.9545×10^{-0}	−0.7884	5.9996×10^{-1}	0.9129
3	2.9079×10^{-0}	1.4086	3.2598×10^{-1}	0.9854
4	1.8562×10^{-0}	0.6864	1.3853×10^{-1}	1.3086
5	6.9086×10^{-1}	1.4687	4.0400×10^{-2}	1.8312
6	2.8930×10^{-1}	1.2747	2.9381×10^{-2}	0.4664
7	1.6919×10^{-1}	0.7797	1.4457×10^{-2}	1.0308
8	1.0582×10^{-1}	0.6796	6.9259×10^{-3}	1.0657

Table 4.6
Energy norm and ℓ_∞ norm errors for Example 4.5.

j	$\|\tilde{e}_j\|_j/\|u_8\|_8$	$\tilde{\beta}_h$	$\|\tilde{e}_j\|_\infty$	$\tilde{\beta}_\infty$
1	5.1600×10^{-0}		1.0628×10^{-0}	
2	$1.0383 \times 10^{+1}$	−1.2495	1.1233×10^{-0}	0.0989
3	4.8834×10^{-0}	1.2185	4.6694×10^{-1}	1.4181
4	3.6378×10^{-0}	0.4503	2.5049×10^{-1}	0.9524
5	1.5514×10^{-0}	1.2664	2.7118×10^{-2}	3.3037
6	6.5449×10^{-1}	1.2639	4.5364×10^{-3}	2.6183
7	2.8868×10^{-1}	1.1898	9.0815×10^{-4}	2.3380
8	1.3864×10^{-1}	1.0621	1.7631×10^{-4}	2.3737

Example 4.4. In this example we take Ω to be the L-shaped domain $(-0.5, 0.5)^2 \setminus [0, 0.5]^2$, $f = g = 0$ and $\psi(x) = 1 - \left[\frac{(x_1+0.25)^2}{0.2^2} + \frac{x_2^2}{0.35^2}\right]$. We solve the discrete obstacle problems using a similar partition as described in Section 2.1. For this example, j is chosen so that it is the level where there are $2^j + 1$ subdivisions in each direction, making $h_j = (2^j + 1 - 1/3)^{-1}$. This allows us to insert an L-shaped element in the vicinity of the reentrant corner as described in Remark 2.4.

From the numerical results in Table 4.5 we observe that $\tilde{\beta}_h$ is approaching $\mathcal{O}(h^\alpha)$ where $\alpha = 0.544$ is the index of elliptic regularity for the L-shaped domain, as predicted by Theorem 3.2.

Since $\Delta^2\psi - f = 0$ for this example, the non-coincidence set is connected [9], which is confirmed by Fig. 4.4.

Example 4.5. In this example we take Ω to be the pentagon $\{x \in (-0.5, 0.5)^2 : x_1 + x_2 < 0.5\}$. We take $f = g = 0$ and $\psi(x) = 1 - 9|x|^2$. We solve the discrete obstacle problems using a similar partition as described in Section 2.1. For this example, j is chosen so that it is the level where there are $2^j + 1$ subdivisions in each direction, making $h_j = (2^j + 1 - 1/3)^{-1}$. This allows us to insert different types of elements near the obtuse vertices of Ω, see Figs. 4.5 and 4.6. The numerical results are reported in Table 4.6.

Since $\Delta^2\psi - f = 0$ in this example, the non-coincidence set is connected [9], which is confirmed by Fig. 4.7, where the discrete coincidence sets also display the correct reflection symmetry.

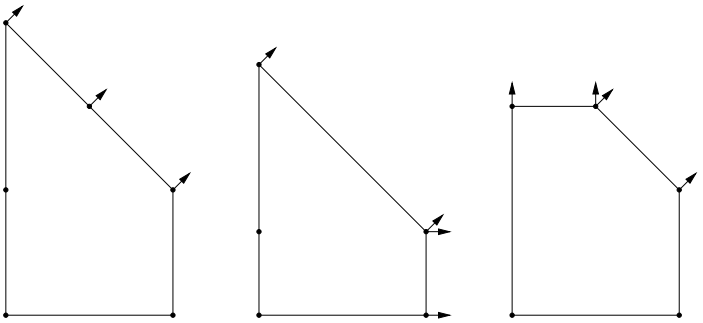

Fig. 4.5. Reference elements for the pentagonal domain.

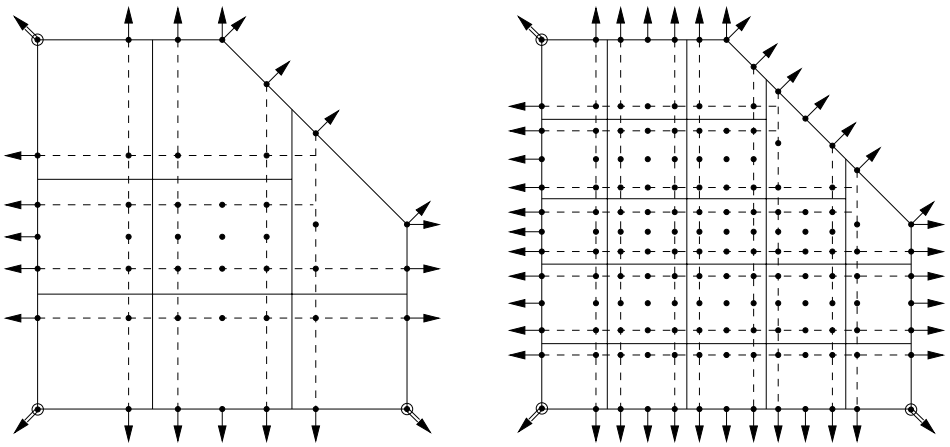

Fig. 4.6. A partition of the pentagonal domain Ω for levels $j = 1$ (left) and $j = 2$ (right). The solid lines separate the different patches Q_j, $j = 1, \ldots, 8$ (left) and Q_j, $j = 1, \ldots, 22$ (right). The dashed lines represent the extension of Q_j by $\delta(h/2)$ on each side. This figure also shows the locations of the degrees of freedom.

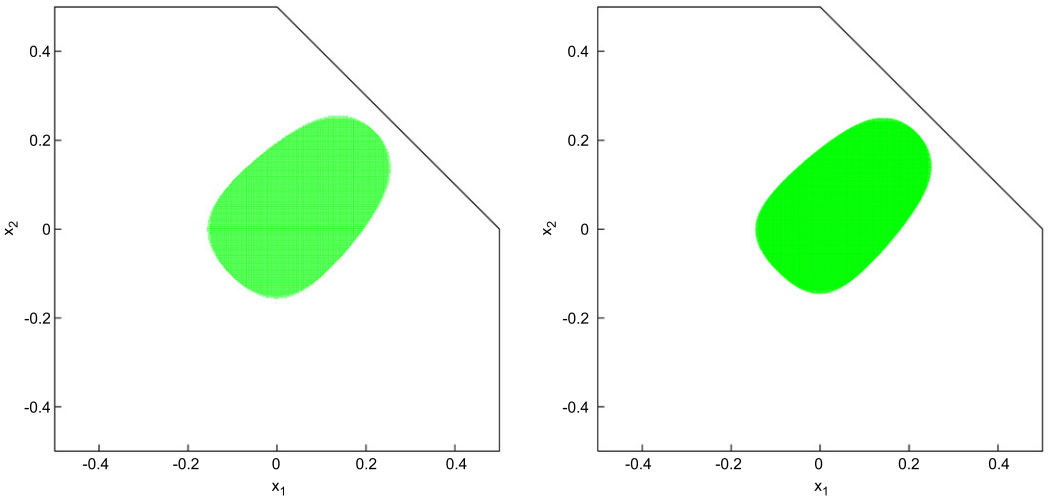

Fig. 4.7. Discrete coincidence set for Example 4.5 for level 7 (left) and level 8 (right).

5. Concluding remarks

We have demonstrated that it is feasible to solve fourth order obstacle problems by a partition of unity method. This method has some nice features that are not shared by other finite element methods. For example, as already mentioned in Remark 2.6, it is possible to use biquadratic polynomials in the local approximation space, instead of using polynomials of individual degrees at least 3 (required for classical C^1 finite element methods). It is also easy to adjust the local approximation

space, as was demonstrated in Example 4.1. In particular it is possible to choose different polynomial spaces on different patches for p-adaptivity.

It is also possible to include certain singular functions in the local approximation spaces to recover optimal convergence for solutions that are less regular. This has been carried out in a related project [35] for the obstacle problem of simply supported plates, where the solution can have strong singularities even on convex polygonal domains.

Another salient feature of the partition of unity method is that in this approach it is easy to construct global C^k approximation spaces for large k, which is not the case for other approaches. Such highly smooth approximation spaces are useful for handling sixth order and eighth order problems that have begun to appear in applications, such as the sixth order phase field crystal model [36] and optimal control problems involving the biharmonic operator that can be solved as eighth order problems [37].

References

[1] J.-L. Lions, G. Stampacchia, Variational inequalities, Comm. Pure Appl. Math. 20 (1967) 493–519.
[2] R. Glowinski, J.-L. Lions, R. Trémolières, Numerical Analysis of Variational Inequalities, North-Holland Publishing Co., Amsterdam, 1981.
[3] D. Kinderlehrer, G. Stampacchia, An Introduction to Variational Inequalities and Their Applications, Society for Industrial and Applied Mathematics, Philadelphia, 2000.
[4] A. Friedman, Variational Principles and Free-Boundary Problems, second ed., Robert E. Krieger Publishing Co. Inc., Malabar, FL, 1988.
[5] R.S. Falk, Error estimates for the approximation of a class of variational inequalities, Math. Comp. 28 (1974) 963–971.
[6] F. Brezzi, W. Hager, P.-A. Raviart, Error estimates for the finite element solution of variational inequalities, Numer. Math. 28 (1977) 431–443.
[7] F. Brezzi, W. Hager, P.-A. Raviart, Error estimates for the finite element solution of variational inequalities, II. Mixed methods, Numer. Math. 31 (1978/79) 1–16.
[8] H.R. Brézis, G. Stampacchia, Sur la régularité de la solution d'inéquations elliptiques, Bull. Soc. Math. France 96 (1968) 153–180.
[9] L.A. Caffarelli, A. Friedman, The obstacle problem for the biharmonic operator, Ann. Sc. Norm. Super. Pisa Cl. Sci. (4) 6 (1979) 151–184.
[10] J. Frehse, Zum Differenzierbarkeitsproblem bei variationsungleichungen höherer Ordnung, Abh. Math. Sem. Univ. Hamburg 36 (1971) 140–149.
[11] J. Frehse, On the regularity of the solution of the biharmonic variational inequality, Manuscripta Math. 9 (1973) 91–103.
[12] H. Blum, R. Rannacher, On the boundary value problem of the biharmonic operator on domains with angular corners, Math. Methods Appl. Sci. 2 (1980) 556–581.
[13] P. Grisvard, Elliptic Problems in Non Smooth Domains, Pitman, Boston, 1985.
[14] M. Dauge, Elliptic Boundary Value Problems on Corner Domains, in: Lecture Notes in Mathematics, vol. 1341, Springer-Verlag, Berlin, Heidelberg, 1988.
[15] V.A. Kozlov, V.G. Maz'ya, J. Rossmann, Spectral Problems Associated with Corner Singularities of Solutions to Elliptic Problems, AMS, Providence, 2001.
[16] S.C. Brenner, L.-Y. Sung, Y. Zhang, Finite element methods for the displacement obstacle problem of clamped plates, Math. Comp. 81 (2012) 1247–1262.
[17] S.C. Brenner, L.-Y. Sung, H. Zhang, Y. Zhang, A quadratic C^0 interior penalty method for the displacement obstacle problem of clamped Kirchhoff plates, SIAM J. Numer. Anal. 50 (2012) 3329–3350.
[18] S.C. Brenner, L.-Y. Sung, H. Zhang, Y. Zhang, A Morley finite element method for the displacement obstacle problem of clamped Kirchhoff plates, J. Comput. Appl. Math. 254 (2013) 31–42.
[19] C.B. Davis, Meshless boundary particle methods for boundary integral equations and meshfree particle methods for plates, Ph.D. Thesis, University of North Carolina at Charlotte, 2011.
[20] H.-S. Oh, C. Davis, J.W. Jeong, Meshfree particle methods for thin plates, Comput. Methods Appl. Mech. Engrg. 209 (2012) 156–171.
[21] I. Babuška, U. Banerjee, J.E. Osborn, Survey of meshless and generalized finite element methods: a unified approach, Acta Numer. 12 (2003) 1–125.
[22] I. Babuška, U. Banerjee, Stable generalized finite element method (SGFEM), Comput. Methods Appl. Mech. Engrg. 201/204 (2012) 91–111.
[23] M. Griebel, M.A. Schweitzer, A particle-partition of unity method, II. Efficient cover construction and reliable integration, SIAM J. Sci. Comput. 23 (2002) 1655–1682.
[24] J.M. Melenk, I. Babuška, The partition of unity finite element method: basic theory and applications, Comput. Methods Appl. Mech. Engrg. 139 (1996) 289–314.
[25] H.-S. Oh, J.G. Kim, W.-T. Hong, The piecewise polynomial partition of unity functions for the generalized finite element methods, Comput. Methods Appl. Mech. Engrg. 197 (2008) 3702–3711.
[26] J.H. Bramble, S.R. Hilbert, Estimation of linear functionals on Sobolev spaces with applications to Fourier transforms and spline interpolation, SIAM J. Numer. Anal. 7 (1970) 113–124.
[27] T. Dupont, R. Scott, Polynomial approximation of functions in Sobolev spaces, Math. Comp. 34 (1980) 441–463.
[28] F.K. Bogner, R.L. Fox, L.A. Schmit, The generation of interelement compatible stiffness and mass matrices by the use of interpolation formulas, in: Proceedings Conference on Matrix Methods in Structural Mechanics, Wright Patterson A.F.B., Dayton, OH, 1965, pp. 397–444.
[29] R.A. Adams, J.J.F. Fournier, Sobolev Spaces, second ed., Academic Press, Amsterdam, 2003.
[30] L. Tartar, An Introduction to Sobolev Spaces and Interpolation Spaces, Springer, Berlin, 2007.
[31] F. Brezzi, L.A. Caffarelli, Convergence of the discrete free boundaries for finite element approximations, RAIRO Anal. Numér. 17 (1983) 385–395.
[32] R.H. Nochetto, A note on the approximation of free boundaries by finite element methods, RAIRO Modél. Math. Anal. Numér. 20 (1986) 355–368.
[33] M. Bergounioux, K. Ito, K. Kunisch, Primal–dual strategy for constrained optimal control problems, SIAM J. Control Optim. 37 (1999) 1176–1194 (electronic).
[34] M. Hintermüller, K. Ito, K. Kunisch, The primal–dual active set strategy as a semismooth Newton method, SIAM J. Optim. 13 (2003) 865–888.
[35] S.C. Brenner, C.B. Davis, L.-Y. Sung, A partition of unity method for a class of fourth order elliptic variational inequalities, 2013, Preprint.
[36] M. Cheng, J.A. Warren, An efficient algorithm for solving the phase field crystal model, J. Comput. Phys. 227 (2008) 6241–6248.
[37] S. Frei, R. Rannacher, W. Wollner, A priori error estimates for the finite element discretization of optimal distributed control problems governed by the biharmonic operator, Calcolo 50 (2013) 165–193.